Supporting Information

Proton-Coupled Electron Transfer Mechanism in Low-Energy Electrochemical CO_2 Desorption from Tiron-Mediated Amine Solutions

Qiuwei $_2$[1], Jan Baeyens[2], Helei Liu[1,*]

[1] Joint International Research Laboratory of Carbon Neutrality System and Engineering Management, Beijing Laboratory for System Engineering of Carbon Neutrality, School of Chemistry and Chemical Engineering, Beijing Institute of Technology, Beijing, 102488, China.

[2] KU Leuven, Department of Chemical Engineering, Process and Environmental Technology Lab, Sint-Katelijne-Waver, Belgium

[*] Email: hl_liu@bit.edu.cn

Additional experimental details
Supplementary text: 4
Supplementary figures: 11

Text 1

Absorption and desorption test

CO_2 absorption was conducted at room temperature by continuously bubbling CO_2 gas into the working chamber of an H-type electrochemical cell. At the beginning of the process, the gas bubbles appeared uniformly fine and dense. As the amine solution approached saturation, the bubble size increased and bubbling became more vigorous. This is attributed to the conversion of free amine to its protonated form, which decreases the viscosity of the solution. The absorption was terminated once saturation was reached, and the CO_2 loading of the solution was determined via acid-base titration using the following equation:

$$\alpha = \frac{(V_4 - V_0) - (V_3 - V_1)}{22.4 \times C_{amine} V_{amine}} \times \frac{273.15}{273.15 + T} \quad \text{(S1)}$$

Where:

V_0 is the initial reading of the measuring cylinder,

V_1 is the initial volume of hydrochloric acid in the burette,

V_3 is the final volume of hydrochloric acid at the end of titration,

V_4 is the final reading of the measuring cylinder,

T is the ambient temperature (used for gas correction),

α is the calculated CO_2 loading (mol CO_2 / mol amine).

Electrochemical CO_2 desorption was also carried out at room temperature by applying a controlled voltage across the H-type cell to drive the proton-coupled electron transfer process. Upon completion, the CO_2 loading was again determined by titration.

The desorption efficiency is calculated based on the difference in CO_2 loading before and after desorption, using the following equation:

$$\gamma = \frac{\alpha_0 - \alpha_1}{\alpha_0} \quad \text{(S2)}$$

Where α_0 represents the CO_2 loading before desorption, and α_1 represents the CO_2 loading after desorption.

The energy consumption of electrochemical CO_2 desorption was evaluated via chronoamperometry. The specific energy consumption per mole of desorbed CO_2 was calculated by integrating the current–voltage profile over time, according to the following

equation:

$$Q = \frac{\int UIt}{(\alpha_0 - \alpha_1) C_{amine} V_{amine} M_{CO_2} \times 1000} \quad \text{(S3)}$$

Here, U represents the real-time voltage measured by the electrochemical workstation, I is the preset current for the experiment, t denotes the electrolysis time, C_{amine} is the concentration of amine in the solution, V_{amine} refers to the volume of the solution in the cell, and M_{CO2} represents the molar mass of CO_2.

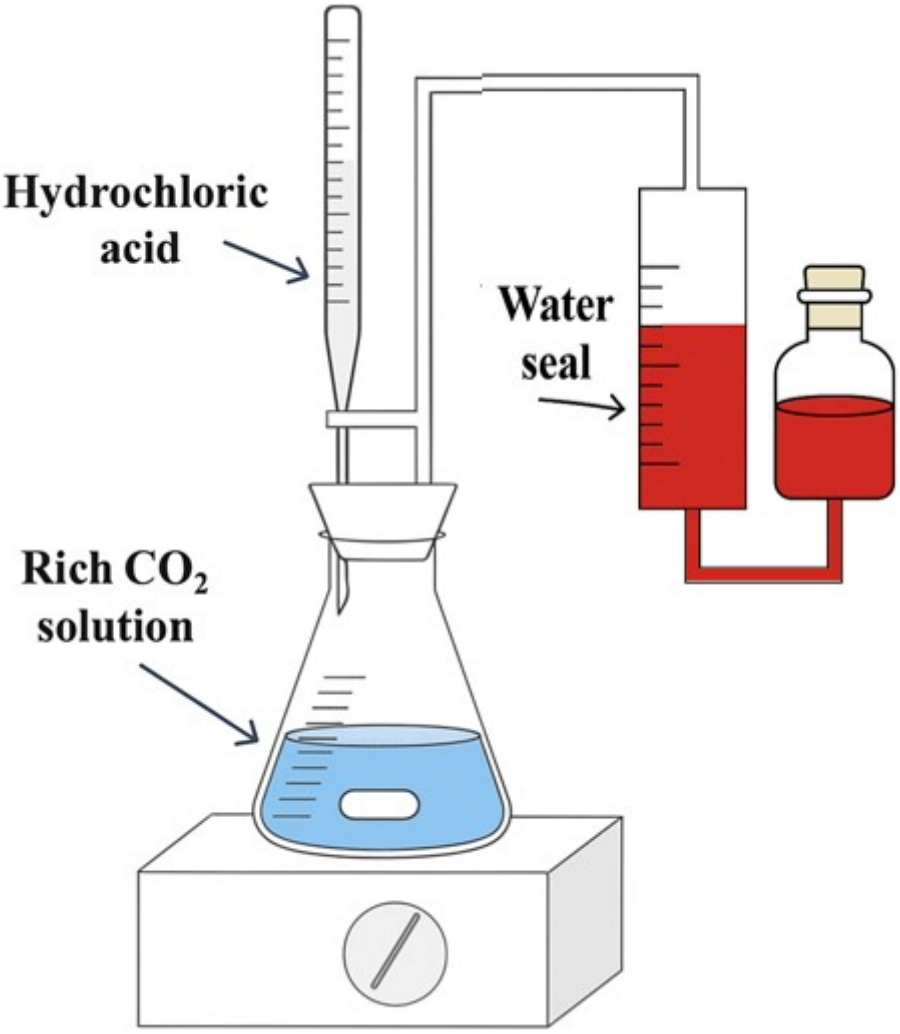

Schematic of the titration device

Text 2

Detailed proton transfer and redox reactions

When the reagents are mixed, the solution undergoes the following reaction:

$$R_3N + H_2O \rightleftharpoons R_3NH^+ + OH^- \quad \text{(S4)}$$

$$QH_2 + OH^- \rightleftharpoons QH^- + H_2O \quad \text{(S5)}$$

Upon CO_2 introduction, absorption occurs:

$$R_3N + H_2O + CO_2 \rightleftharpoons R_3NH^+ + {}^{HCO}{}_3^- \quad \text{(S6)}$$

The desorption reaction (oxidation) process as follow:

$$QH^- - 2e^- = Q + H^+ \quad \text{(S7)}$$

$$QH_2 - 2e^- = Q + 2H^+ \quad \text{(S8)}$$

$$H^+ + {}^{HCO}{}_3^- = H_2O + CO_2 \quad \text{(S9)}$$

The solvent regeneration (reduction) process as follow:

$$Q + 2e^- = Q^{2-} \quad \text{(S10)}$$

$$Q^{2-} + H_2O = QH^- + OH^- \quad \text{(S11)}$$

$$QH^- + H_2O = QH_2 + OH^- \quad \text{(S12)}$$

$$Q^{2-} + R_3NH^+ = QH^- + R_3N \quad \text{(S13)}$$

$$QH^- + R_3NH^+ = QH_2 + R_3N \quad \text{(S14)}$$

$$R_3NH^+ + OH^- = R_3N + H_2O \quad \text{(S15)}$$

Text 3

Calculation of double-layer capacitance

To evaluate the electrochemical surface area of modified electrodes and their interfacial ion transport behavior with the solvent, the double-layer capacitance (Cdl) was determined using cyclic voltammetry (CV) in the non-Faradaic potential region. Cdl serves as an indicator of the interfacial structure between the electrode and electrolyte, and its magnitude correlates with the density of surface area, interfacial wettability, and the uniformity of local ion distribution.

In this study, CV was performed at five scan rates (10, 20, 50, 80, and 100 mV/s) within the non-Faradaic potential windows specific to each electrode. Due to slight differences in the redox potential ranges among electrodes, the selected non-Faradaic regions were accordingly adjusted. The capacitive current at the maximum potential was extracted and plotted as a function of scan rate. The slope of the resulting linear fit corresponds to the Cdl, according to the relationship:

$$i = Cdl \times v \tag{S16}$$

where i is the capacitive current (typically taken at open-circuit voltage), and v is the scan rate. A higher Cdl indicates a larger electrochemically active surface area or improved wettability at the electrode–electrolyte interface.

Text 4

Molecular Dynamics (MD) Simulations

Molecular dynamics simulations were performed to investigate the structural and dynamic behavior of MDEA and DEEA aqueous systems. The molecular geometries of both amines were first optimized using the Gaussian 16 software package [1] at the M06-2X/6-31G(d,p) level of theory. The electrostatic potential (ESP) was subsequently calculated at the TPSSh/def2-TZVP level, and atomic partial charges were derived using the restrained electrostatic potential (RESP) fitting method [2].

The General AMBER Force Field (GAFF) was applied for all simulations, as it is well-suited for modeling organic molecules. All MD simulations were carried out using GROMACS version 2021.3 [3]. Simulation boxes were constructed by placing eight solute molecules (MDEA or DEEA) in a cubic water box of 5 nm edge length under periodic boundary conditions, corresponding to a solute concentration of approximately 0.1 mol/L, consistent with experimental conditions.

Each system underwent a 20 ns equilibrium MD simulation in the NPT ensemble at 300 K. Prior to production runs, energy minimization was performed using the steepest descent algorithm. This was followed by pre-equilibration in the NVT and NPT ensembles for 10 ps and 100 ps, respectively, using the Berendsen thermostat and barostat [4]. During the production stage, temperature and pressure were maintained using the velocity-rescaling thermostat [5] and Parrinello–Rahman barostat [6], respectively. The classical Newtonian equations of motion were integrated using the leap-frog algorithm with a time step of 2 fs. Long-range electrostatic interactions were treated using the Particle Mesh Ewald (PME) method [7,8].

DFT calculation.

Density functional theory (DFT) [9] computations were performed using the Vienna Ab Initio Simulation Package (VASP) [10, 11]. The projector-augmented wave (PAW) method [12] characterized the interaction between valence electrons and ions. Exchange-correlation effects within the Kohn-Sham equation [13] were described via the Perdew-Burke-Ernzerhof (PBE) functional under the generalized gradient approximation (GGA) [14]. A plane-wave basis set with a 400 eV kinetic energy cutoff expanded the wavefunctions. For slab calculations, Brillouin zone sampling utilized a 2×2×1 Mokhorst-Pack k-point grid [15]. Geometry optimization convergence criteria were set at 0.02 eV/Å for atomic forces and 10^{-4} eV for total energies, with a stricter limit of 10^{-8} eV adopted for SCF iteration energy convergence.

The reaction model for practical experiments involved placing CH_2OH and $P(OH)_2O$ onto a monolayer graphene surface. Adsorbed molecules were represented as $C_6H_2O_8S_2^{2-}$ with two pseudo-hydrogen atoms added to neutralize charge. To minimize image interference, a minimum 20 Å vacuum spacing was applied normal to the surface for all slab models and in all directions for nanoclusters. The Gibbs free energy of adsorption (ΔG) was calculated using the following formula:

$$\Delta G = E_{ad} + \Delta ZPE - T\Delta S \quad \text{(S17)}$$

where E_{ad} is the adsorption energy defined by:

$$E_{ad} = E_{surface+adsorbate} - E_{surface} - E_{adsorbate} \quad \text{(S18)}$$

ΔZPE and ΔS are the changes in zero-point energy and entropy during adsorption [16,17].

PCET	Proton-coupled electron transfers
QH2	Trion
MDEA	N-Methyldiethanolamine
DEEA	N,N-Diethylethanolamine
U-GF	Untreated graphite felt
H-GF	Heat treatment graphite felt
A-GF	Acid treatment graphite felt
P-GF	Phosphorus doped graphite felt
CV	Cyclic voltammetry
Cdl	Double-layer capacitance

Table S1. List of Abbreviations in the Text

Table S2. Comparison of energy consumption for CO_2 desorption among different regeneration technologies.

Technology Strategy	Mediator / Method	Driving Energy	Energy Consumption (GJ ton^{-1} CO_2)	Reference
Solid Acid Catalyst	Γ-Al_2O_3 / H-ZSM-5	Thermal	3.2 – 3.9	[18]
Inhibited Amine	MEA + Inhibitor	Thermal	3.12	[19]
Sterically Hindered Amine	KS-2	Thermal	3.0	[20]
Phase-change Solvent	MDEA-TETA / PZ	Thermal	2.52 – 2.55	[21, 22]
EMAR	Cu^{2+}	Thermal + Electric	1.02~1.82	[23, 24]
Redox-carriers	quinones	Electric	1.1~4.5	[25,26]
Bipolar Membrane (BPM)	Electrodialysis	Electric	1.18 – 4.5	[27, 28]
pH-swing Electrodialysis	CO_2/H_2 Mix	Electric	2.0 – 2.27	[29, 30]
Redox Carrier (PCET)	DSPZ	Electric	1.4	[31]
Redox Carrier (PCET)	H_2/AQDS	Electric	1.12	[32]
Redox Carrier (PCET)	1,8-ESP	Electric	0.82 – 1.25	[33]
This Work (PCET)	**QH_2 / P-GF**	**Electric**	**0.62**	**This Work***

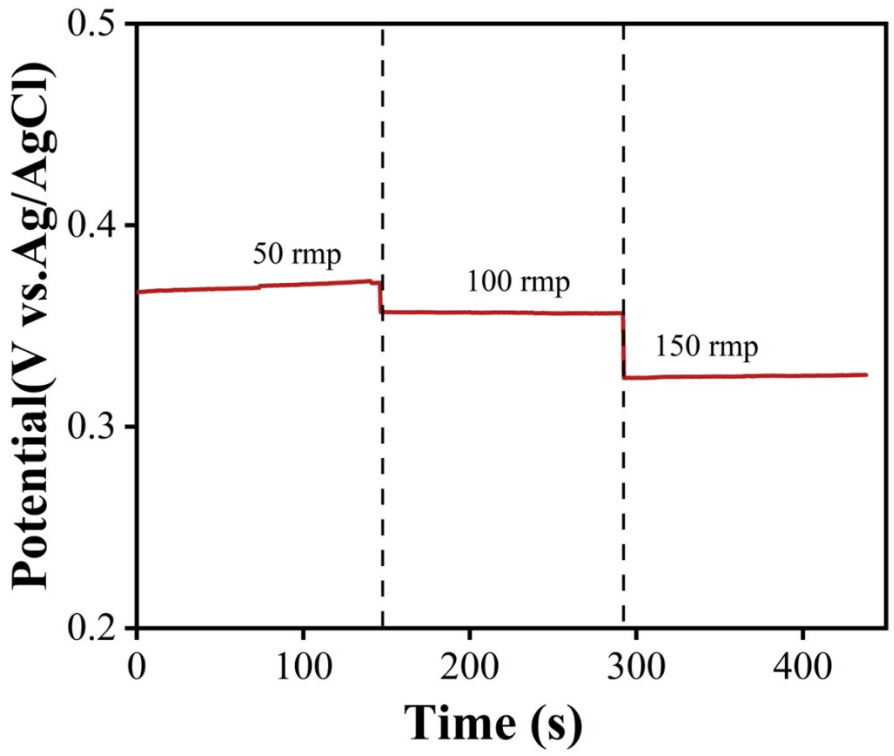

Figure S1. Potential response under different stirring speeds during constant current electrochemical oxidation.

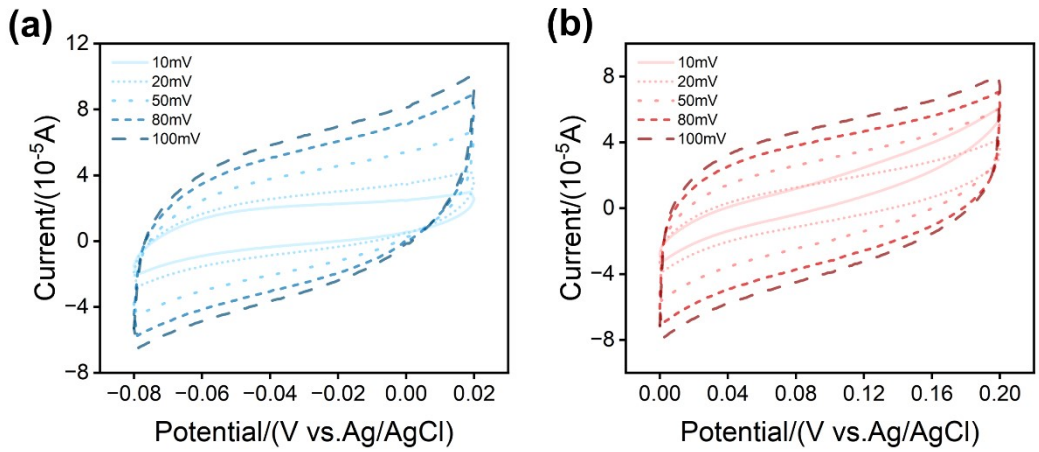

Figure S2. Non-Faradaic CV curves under untreated electrode. (a) MDEA. (b) DEEA.

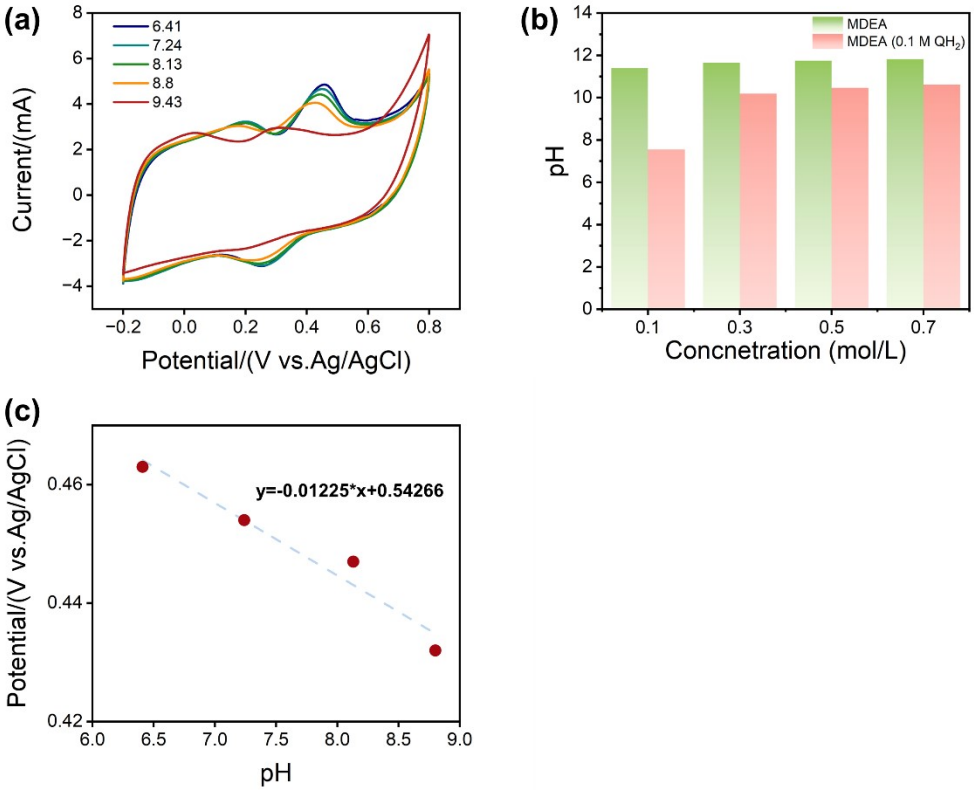

Figure S3. pH-dependent electrochemical characteristics of MDEA solutions. (a) Cyclic voltammograms of MDEA solutions at different pH values under N_2 atmosphere, scanned at 10 mV s^{-1}. (b) Measured pH of MDEA solutions at various concentrations and in QH_2-containing systems (0.1 M). (c) Peak Potential as a Function of pH in MDEA Solution.

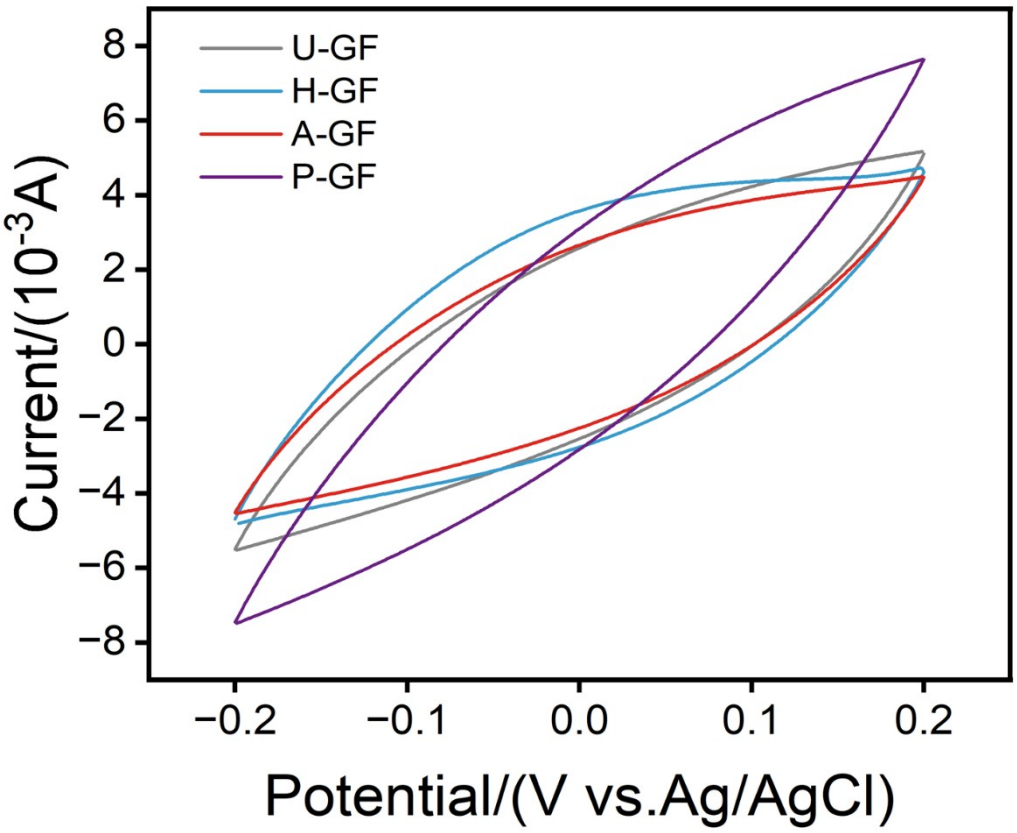

Figure S4. Non-Faradaic CV curves of MDEA systems under different electrode modifications.

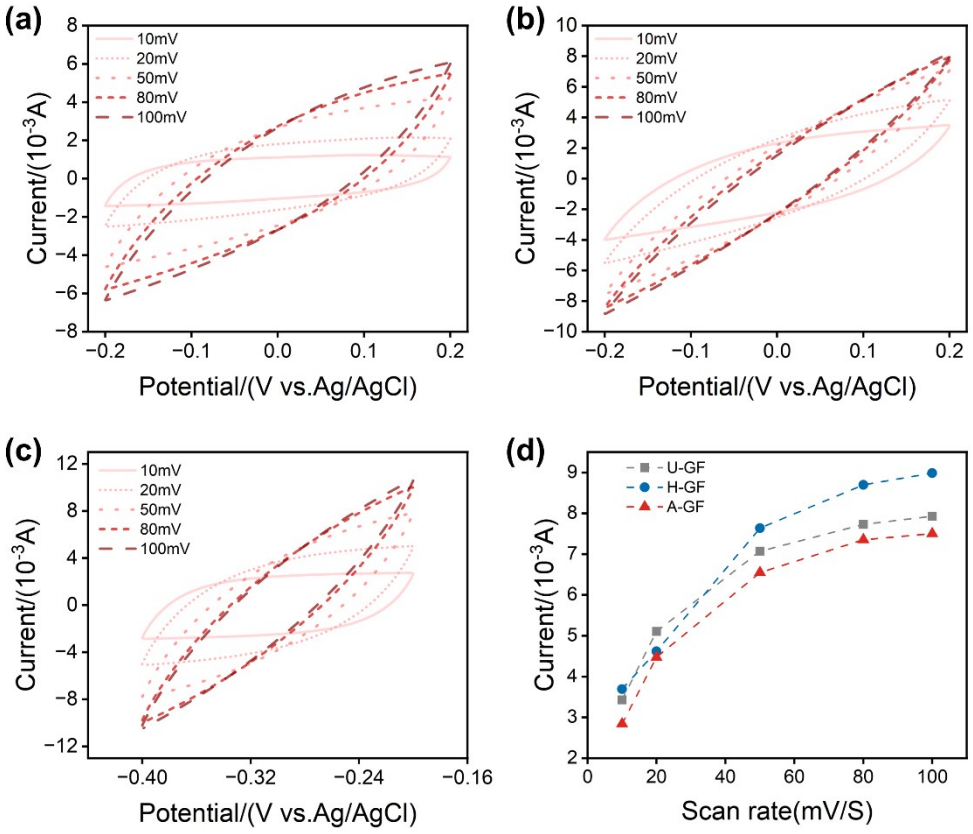

Figure S5. Non-Faradaic CV curves of DEEA systems under different electrode modifications. (a) Heat-treated electrode; (b) Acid-treated electrode; (c) P-doped electrode; (d) Corresponding current response versus scan rate used for double-layer capacitance (Cdl) calculation.

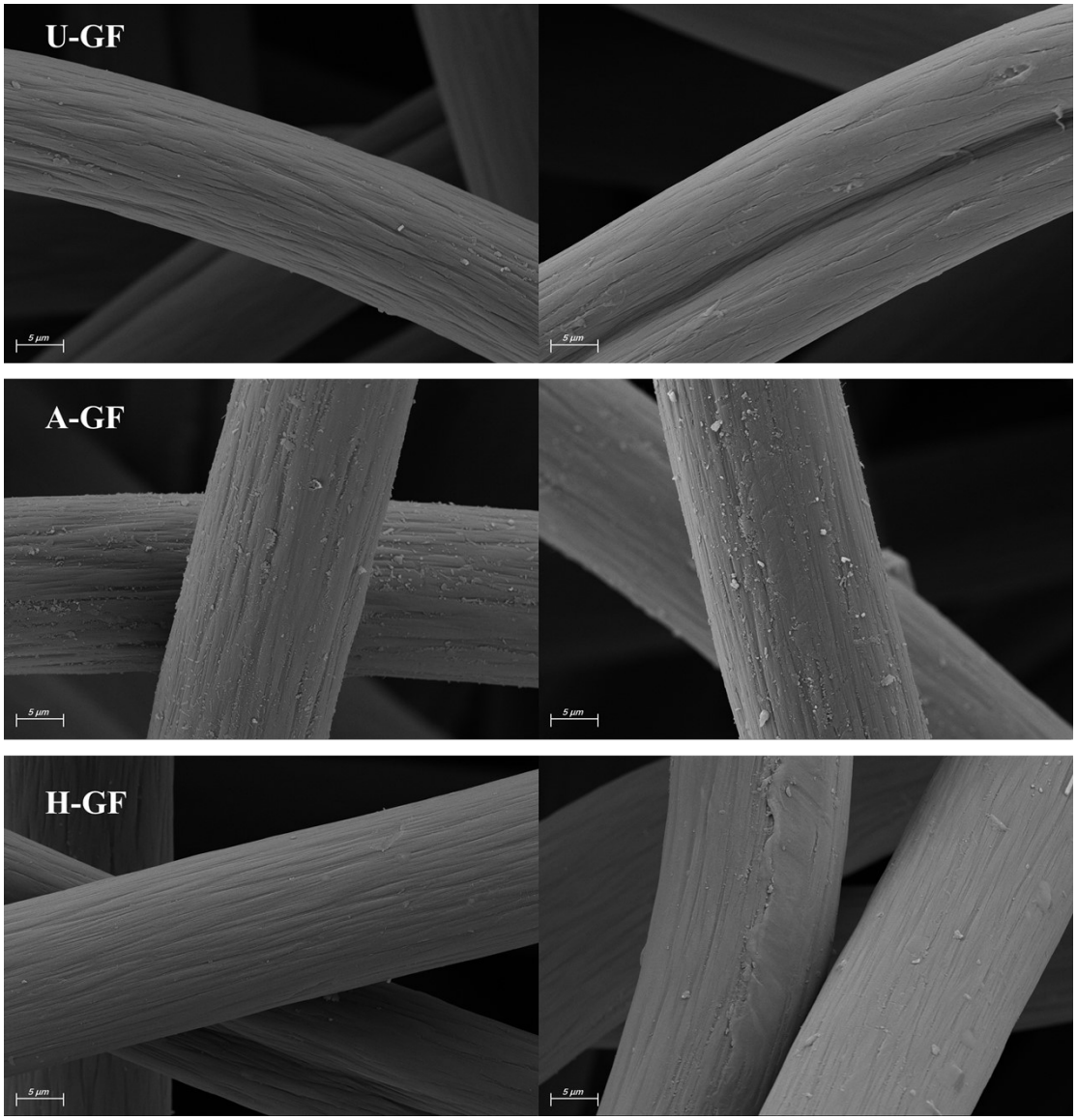

Figure S6. SEM images of untreated, acid-treated, and heat-treated graphite felt electrodes at different magnifications. Heat treatment does not effectively modify the internal carbon felt

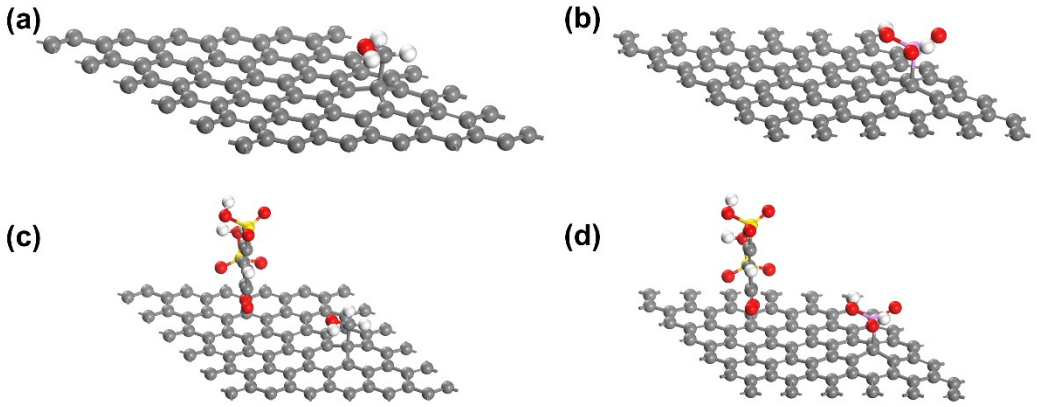

Figure S7. DFT-calculated surface models used for PDOS and adsorption energy analysis. (a) Untreated carbon felt surface model. (b) P-doped carbon felt surface model. (c) U-GF surface model with Q molecule adsorption site indicated. (d) P-doped surface model with Q molecule adsorption site indicated.

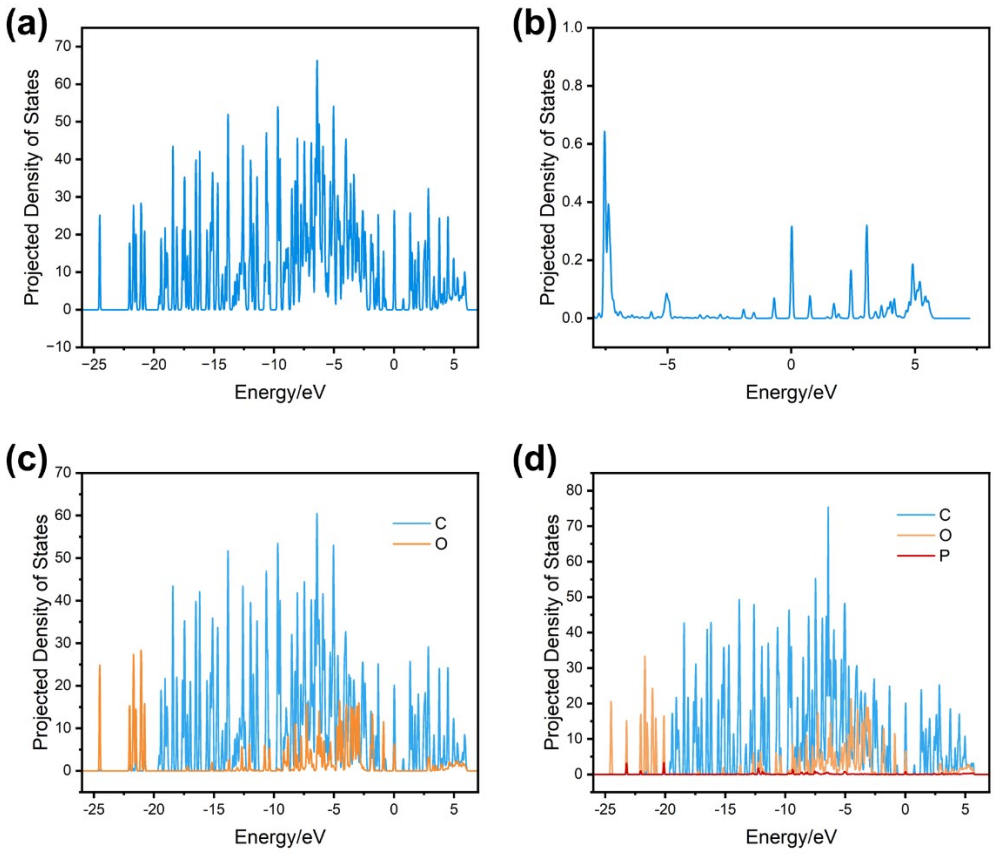

Figure S8. Projected density of states (PDOS) analysis of CH_2–OH and P–OH functional groups. (a) Total PDOS of all atoms in CH_2–OH as a function of energy. (b) s-orbital PDOS of P atoms in P–OH functional groups. (c) Atom-resolved total PDOS of individual C and O atoms in CH_2–OH. (d) Total PDOS of C, O, and P atoms in P–OH.

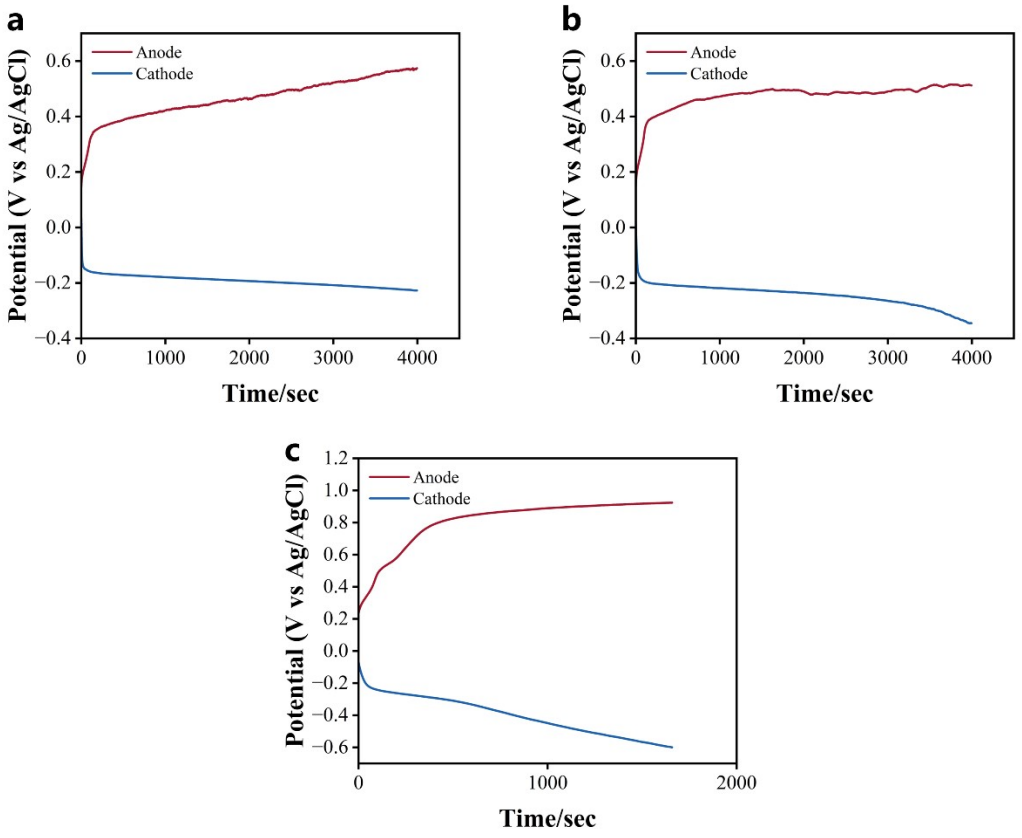

Figure S9. Original potential profiles recorded over multiple desorption cycles in MDEA solution using a heat-treated electrode. (a) First cycle. (b) Second cycle. (c) Third cycle. Electrostatic technique was used in the experiments to obtain the power consumption by keeping the current constant and recording the potential changes. The electrode used for electrochemical desorption was a 2×2 cm^2 electrode with a current of 40 mA (10 mA/cm^2). The energy consumption for electrochemical CO_2 desorption was calculated using Equation S3. Due to significant differences in the reduction times of various electrodes, a uniform sampling duration of 4000 s was selected. The amount of CO_2esorbed during this period, determined by titration, was used for the energy consumption calculation.

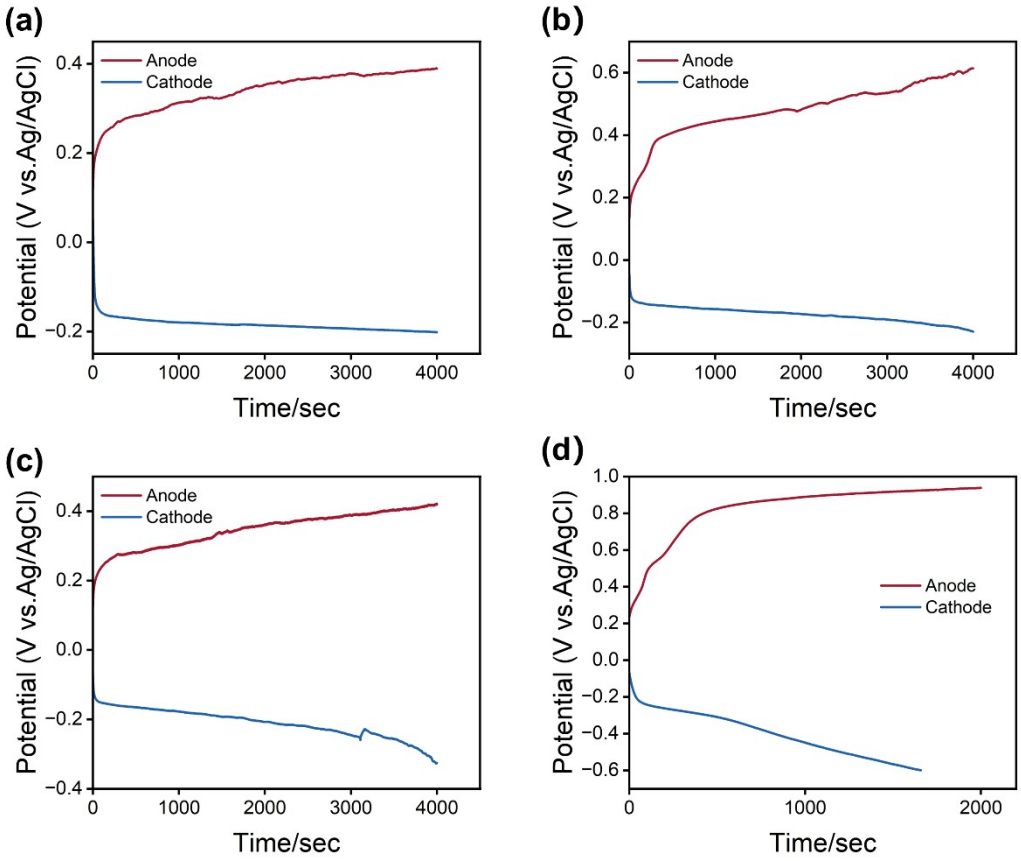

Figure S10. Original potential profiles recorded over multiple desorption cycles in MDEA solution using a acid-treated electrode. (a) First cycle. (b) Second cycle. (c) Third cycle. (d) Fourth cycle.

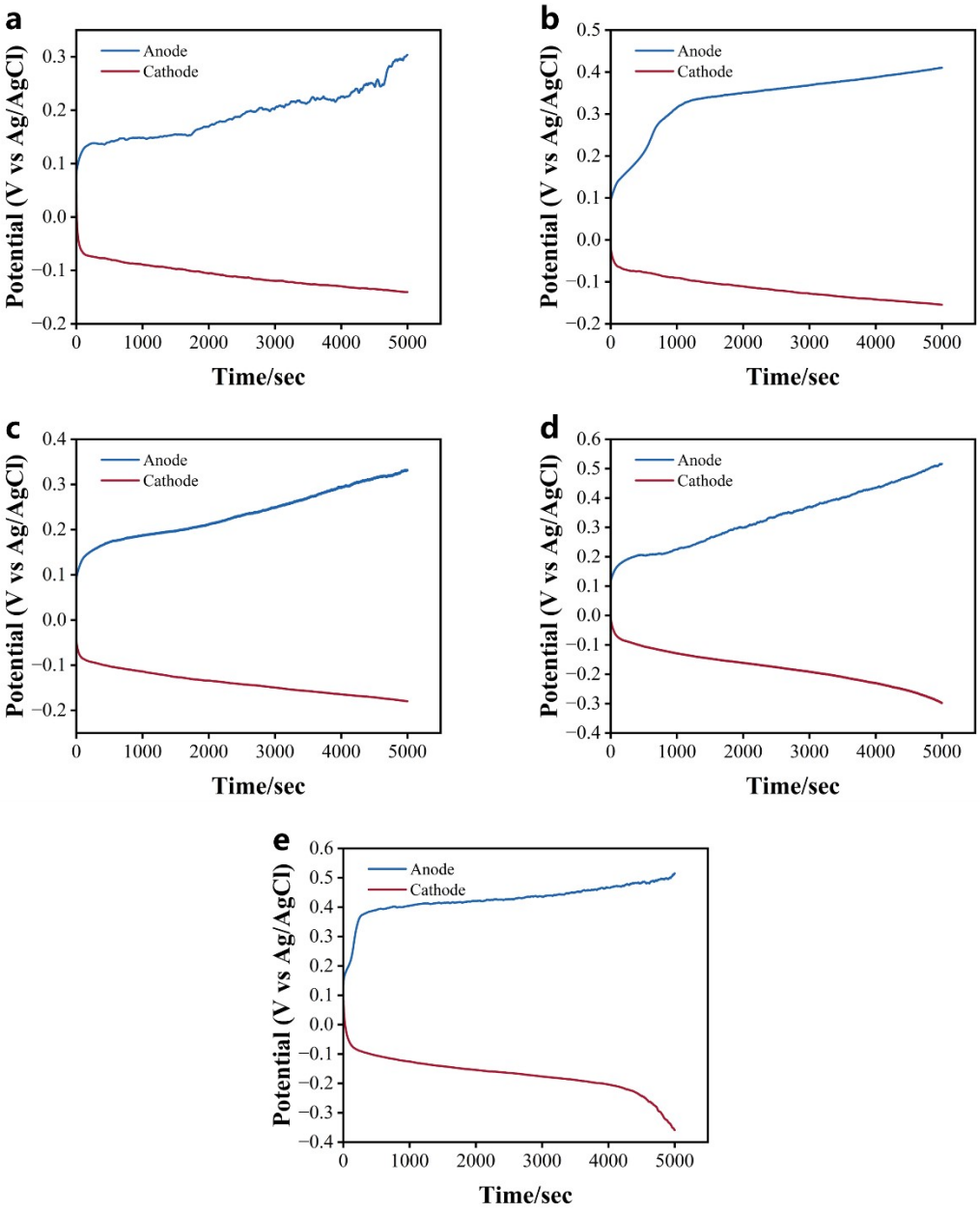

Figure S11. Original potential profiles recorded over multiple desorption cycles in MDEA solution using a P-doping electrode. electrodes. (a) First cycle. (b) Second cycle. (c) Third cycle. (d) Fourth cycle. (e) Fifth cycle.

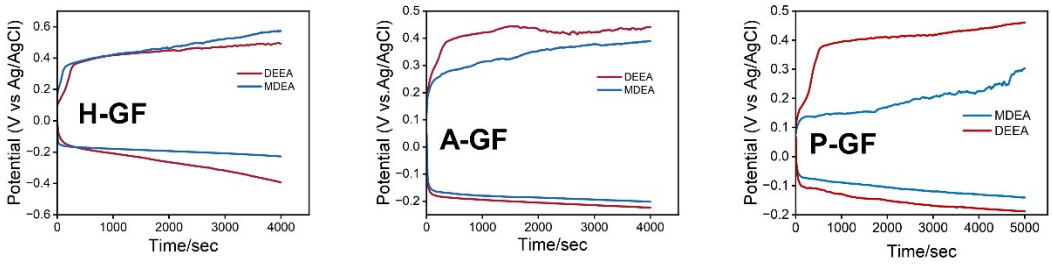

Figure S12. Initial cycling voltage curves of different amine solutions in different electrodes

References

[1] Frisch M J, Trucks G W, Schlegel H B, et al. Gaussian 16 Rev. C.01[Z]. Wallingford, CT. 2016

[2] Schauperl M, Nerenberg P S, Jang H, et al. Force Field Partial Charges with Restrained Electrostatic Potential 2 (RESP2)[J]. Chemrxiv, 2019, DOI: 10.26434/chemrxiv.10072799.

[3] Hess B, Kutzner C, Van Der Spoel D, et al. 4: Algorithms for Highly Efficient, Load-Balanced, and Scalable Molecular Simulation[J]. 2008, 4: 435-447.

[4] Berendsen H J C, Postma J P M, Van Gunsteren W F, et al. Molecular Dynamics with Coupling to An External Bath[J]. Journal of Chemical Physics, 1984, 81(8): 3684-3690.

[5] Bussi G, Donadio D, Parrinello M. Canonical Sampling through Velocity Rescaling[J]. Journal of Chemical Physics, 2007, 126(1): 014101.

[6] Parrinello M, Rahman A. Polymorphic Transitions in Single Crystals: A New Molecular Dynamics Method[J]. Journal of Applied Physics, 1981, 52(12): 7182-7190.

[7] Essmann U, Perera L, Berkowitz M L, et al. A Smooth Particle Mesh Ewald Method [J]. Journal of Chemical Physics, 1995, 103(19): 8577-8593.

[8] Darden T, York D, Pedersen L. Particle mesh Ewald: An N·log(N) Method for Ewald Sums in Large Systems[J]. Journal of Chemical Physics, 1993, 98(12): 10089-10092.

[9] W. Kohn, L.J. Sham, Self-Consistent Equations Including Exchange and Correlation Effects, Physical Review 140(4A) (1965) A1133-A1138.

[10] G. Kresse, J. Furthmüller, Efficient iterative schemes for ab initio total-energy calculations using a plane-wave basis set, Physical Review B 54(16) (1996) 11169-11186.

[11] G. Kresse, D. Joubert, From ultrasoft pseudopotentials to the projector augmented-wave method, Physical Review B 59(3) (1999) 1758-1775.

[12] J.P. Perdew, J.A. Chevary, S.H. Vosko, K.A. Jackson, M.R. Pederson, D.J. Singh, C. Fiolhais, Atoms, molecules, solids, and surfaces: Applications of the generalized gradient approximation for exchange and correlation, Physical Review B 46(11) (1992) 6671-6687.

[13] J.P. Perdew, K. Burke, M. Ernzerhof, Generalized Gradient Approximation Made Simple, Physical Review Letters 77(18) (1996) 3865-3868.

[14] P.E. Blöchl, Projector augmented-wave method, Physical Review B 50(24) (1994) 17953-17979.

[15] H.J. Monkhorst, J.D. Pack, Special points for Brillouin-zone integrations, Physical Review B 13(12) (1976) 5188-5192.

[16] J.K. Nørskov, J. Rossmeisl, A. Logadottir, L. Lindqvist, J.R. Kitchin, T. Bligaard, H. Jónsson, Origin of the Overpotential for Oxygen Reduction at a Fuel-Cell Cathode, The Journal of Physical Chemistry B 108(46) (2004) 17886-17892.

[17] V. Wang, N. Xu, J.-C. Liu, G. Tang, W.-T. Geng, VASPKIT: A user-friendly interface facilitating high-throughput computing and analysis using VASP code, Computer Physics Communications 267 (2021) 108033.

[18] Liang Z, Idem R, Tontiwachwuthikul P, et al. Experimental study on the solvent regeneration of aCO_2-loaded MEA solution using single and hybrid solid acid catalysts[J]. AIChE Journal, 2016, 62(3): 753-765.

[19] Ghg I. Improvement in power generation with post-combustion capture of CO_2 [R]. United Kingdom: IEA Greenhouse Gas R&D Programme, 2004.

[20] Gibbins J, Crane R. Scope for reductions in the cost of CO_2 capture using flue gas scrubbing with amine solvents[J]. Proceedings of the Institution of Mechanical Engineers, Part A: Journal of Power and Energy, 2004, 218(4): 231-239.

[21] Amann J-M G, Bouallou C. CO_2 capture from power stations running with natural gas (NGCC) and pulverized coal (PC): Assessment of a new chemical solvent based on aqueous solutions of Nmethyldiethanolamine + triethylene tetramine[J]. Energy Procedia, 2009, 1(1): 909-916.

[22] Oexmann J, Hasenbein C, Kather A. Semi-empirical model for the direct simulation of power plant with integrated post-combustion CO_2 capture processes by wet chemical absorption[J]. Energ procedia, 2011, 4: 1276-1285.

[23] Wang M, Rahimi M, Kumar A, et al. Flue gas CO_2 capture via electrochemically mediated amine regeneration: System design and performance[J]. Applied energy, 2019, 255: 113879.

[24] Wang M, Herzog H J, Hatton T A. CO_2 capture using electrochemically mediated amine regeneration[J]. Industrial & Engineering Chemistry Research, 2020, 59(15): 7087-7096.

[25] Diederichsen K M, Liu Y, Ozbek N, et al. Toward solvent-free continuous-flow electrochemically mediated carbon capture with high-concentration liquid quinone chemistry[J]. Joule, 2022, 6(1): 221-239.

[26] Voskian S, Hatton T A. Faradaic electro-swing reactive adsorption for CO_2 capture[J]. Energy & Environmental Science, 2019, 12(12): 3530-3547.

[27] Valluri S, Kawatra S K. Reduced reagent regeneration energy for CO_2 capture with bipolar membrane electrodialysis[J]. Fuel Processing Technology, 2021, 213: 106691.

[28] Eisaman M D, Alvarado L, Larner D, et al. CO_2 separation using bipolar membrane electrodialysis[J]. Energy & Environmental Science, 2011, 4(4): 1319-1328.

[29] Taniguchi I, Ioh D, Fujikawa S, et al. An alternative carbon dioxide capture by electrochemical method[J]. Chemistry Letters, 2014, 43(10): 1601-1603.

[30] Nagasawa H, Yamasaki A, Iizuka A, et al. A new recovery process of carbon dioxide from alkaline carbonate solution via electrodialysis[J]. AIChE Journal, 2009, 55(12): 3286-3293.

[31] Jin S, Wu M, Jing Y, et al. Low energy carbon capture via electrochemically induced pH swing with electrochemical rebalancing[J]. Nature Communications, 2022, 13(1): 2140.

[32] Liu T, Wang Y, Wu Y, et al. Continuous decoupled redox electrochemical CO_2 capture[J]. Nature Communications, 2024, 15(1): 10920.

[33] Pang S, Jin S, Yang F, et al. A phenazine-based high-capacity and high-stability electrochemical CO_2 capture cell with coupled electricity storage[J]. Nature Energy, 2023, 8(10): 1126-1136.